Journal of Crystal Growth 354 (2012) 20–26

Contents lists available at SciVerse ScienceDirect

Journal of Crystal Growth

journal homepage: www.elsevier.com/locate/jcrysgro

Ring crystals of oligonucleotides: Growth stages and X-ray diffraction studies

Pradeep K. Mandal [a], Arun Richard Chandrasekaran [b], Bharath Raj Madhanagopal [c], Sarkarai Venkadesh [a], Namasivayam Gautham [a,*]

[a] C.A.S. in Crystallography and Biophysics, University of Madras, Guindy, Chennai 600025, India
[b] Department of Chemistry, 100 Washington Square East, New York University, NY 10003, USA
[c] Department of Biology, Indian Institute of Science Education and Research, Pashan, Pune 411021, India

ARTICLE INFO

Article history:
Received 22 December 2011
Received in revised form
21 May 2012
Accepted 23 May 2012
Communicated by M. Fleck
Available online 2 June 2012

Keywords:
A1. Biocrystallization
A1. Crystal morphology
A1. Crystal structure
A1. X-ray diffraction

ABSTRACT

The hexamer duplex d(CACGCG).d(CGCGTG) produces unusual hexagonal ring shaped crystals when crystallized in the presence of cobalt hexammine chloride. Observation of the growth of these crystals over a period of about 6 days indicated that this morphology resulted from radial dissolution of the crystal from the center of the well-formed hexagonal plates. X-ray diffraction studies were carried out for crystals of four stages in the ring crystal morphology. The structure of the DNA in all four crystals was the Z type DNA double helix. The packing mode of the Z DNA duplex in all four crystal structures was that of the 'spermine' form. The crystal morphology changes from hexagonal plates to hexagonal rings without any apparent change in the molecular structure of the oligonucleotide or helical packing of the duplexes.

1. Introduction

Apart from the fundamental role as a carrier of genetic information, DNA continues to draw significant study purely as a component of molecular systems with complex order [1]. DNA can be condensed by a variety of methods [2,3] yielding a spectrum of liquid crystalline order. The crystalline ordering of DNA is quite a complex problem due to microscopic frustration introduced by the hexagonal packing of helical molecules. At high packing densities of crystalline DNA, the interactions between neighboring helices are complex, involving a combination of electrostatic, hydrogen bonding, steric and ion-mediated forces [1]. Based on generic symmetry considerations of helical polymer arrays, nascent crystalline ground states fall largely into two categories: unfrustrated or weakly frustrated; and a highly frustrated state [1].

Ring shaped crystals of organic and inorganic substances have previously been reported [4–8]. As to their growth mechanisms, various hypotheses have been advanced in order to explain the formation of these particular morphologies [8,9]. Some authors put forward the idea that the hollow forms are strictly related to the initial form of the nuclei (e.g., ring-like nuclei). Others claim that the hollow growth mechanism is of a spiral type and depends on the presence, in a point of the growing interface, of a screw dislocation from which the hollow form develops via a layer-like growth process [5,10,11].

An earlier report from our laboratory [12] described the occurrence of ring-shaped crystals of the non-self-complementary hexameric sequences d(CGCGCA).d(TGCGCG) and d(CGCACG).d(CGTGCG). Here, we report observations of the entire growth process of ring shaped crystals of another, but similar sequence d(CACGCG).d(CGCGTG) and the X-ray crystal structures of the ring crystals at various stages of the growth process.

2. Experimental procedures

2.1. Crystallization

Poly acrylamide gel electrophoresis purified hexanucleotides d(CACGCG) and d(CGCGTG) were purchased from M/s Microsynth, Switzerland. The two cross-complementary sequences were annealed to form the duplex by heating an equimolar mixture of the two to 343 K over a period of 1 h, and then allowing the solution to cool to room temperature over a period of 4 h. The cooled solution was stored at 283 K and used for crystallization. Table 1 summarizes the different conditions under which crystallization of this sequence was attempted. The ring crystals were grown by the hanging drop vapor-diffusion method at 293 K from drops containing 1 mM DNA, 50–75 mM sodium cacodylate trihydrate buffer (pH 6.9), 0.5–0.75 mM cobalt hexammine chloride, and 0.75 mM spermine, equilibrated against 50% methyl pentane diol (MPD).

* Corrsesponding author. Tel.: +91 44 2220 2774; fax: +91 44 2230 0122.
E-mail address: n_gautham@hotmail.com (N. Gautham).

0022-0248/$ - see front matter © 2012 Elsevier B.V. All rights reserved.
http://dx.doi.org/10.1016/j.jcrysgro.2012.05.029

Table 1
Summary of crystallization conditions attempted with d(CACGCG)·d(CGCGTG).

Sl. No.	Hanging drop components	Reservoir (MPD) (%)	Observation
Screening			
1.	DNA*: 1.00 mM Buffer#: 50 mM $Co(NH_3)_6Cl_3$: 0.30–0.45 mM Spermine: 0.75–1.00 mM	40–50	Clear drop
2	DNA*: 1.00 mM Buffer#: 50–75 mM $Co(NH_3)_6Cl_3$: 0.5–0.75 mM Spermine: 0.75–1.00 mM	40–50	Large number of ring-shaped crystals
3	DNA*: 1.00–1.25 mM Buffer#: 50–75 mM $Co(NH_3)_6Cl_3$: 1.0–1.25 mM Spermine: 0.75–1.00 mM	40–50	Precipitate
4.	DNA*: 1.00 mM Buffer#: 50 mM $BaCl_2$: 5.00 mM Spermine: 0.5 mM	50	Hexagonal crystals with no ring formation [PDB ID: 4E60]
5.	DNA*: 1.00 mM Buffer#: 50 mM $BaCl_2$: 10.00 mM Spermine: 0.5 mM	30	Orthorhombic crystals [PDB ID: 4E2R]
6.	DNA*: 1.00 mM Buffer#: 50 mM $MnCl_2$: 1.00 mM Spermine: 1.00 mM	50	Hexagonal crystals with no ring formation [PDB ID: 4DY8]
7.	DNA*: 1.00 mM Buffer#: 50 mM $MnCl_2$: 10.00 mM Spermine: 1.00 mM	50	Monoclinic crystals [PDB ID: 4DWY]
Optimization			
8.	DNA*: 1 mM Buffer#: 50 mM $Co(NH_3)_6Cl_3$: 0.75 mM Spermine: 0.75 mM	50	Large number of ring-shaped crystals
9.	DNA*: 1 mM Buffer#: 75 mM $Co(NH_3)_6Cl_3$: 0.5 mM Spermine: 0.75 mM	50	Large number of ring-shaped crystals

DNA*=d(CACGCG).d(CGCGTG).
Buffer#=sodium cacodylate trihydrate (pH=6.9).

2.2. Optical microscopy

Optical examination of the crystals and documentation of various growth stages was carried out using a Reichert Polyvar Met2 microscope. The crystallization experiment was placed on the observation stage of the microscope as soon as it was set up, and left undisturbed. Observations were made every 1 h and photographs were taken. In subsequent trials, depending on the growth rate, observations were made every half an hour or every 2 h.

2.3. X-ray data collection

Crystals at the following four stages of the crystal growth process were transferred to a 50% solution of MPD, thereby arresting the growth process at these stages. The four stages are (i) hexagonal crystals; (ii) hexagonal crystals with spots on the hexagonal plane; (iii) hexagonal crystals with intense spots and depressions on the hexagonal plane; and (iv) fully formed ring crystals. The crystals were preserved in the solution at 293 K. They were later mounted on loops and used for cryo-crystallography.

For data collection at 100 K, the crystals were flash-cooled in liquid nitrogen. X-ray diffraction data for stages (i), (iii) and (iv) were collected in-house on a MAR Research Imaging Plate system using Cu Kα radiation (λ=1.5418 Å) generated by a Microstar rotating anode X-ray generator (Bruker AXS) operated at 45 kV and 60 mA, at the G.N. Ramachandran X-ray Diffraction Facility, University of Madras, Chennai, India. X-ray diffraction data for stage (ii) was collected on a MAR Research CCD Detector using the XRD-1 beam line in Elletra Synchrotron Radiation Facility, Italy, with a wavelength of 1.54 Å. The intensity data were collected for every 1° rotation of ϕ axis between 150 and 200 mm detector-to-crystal distances. The exposure time was maintained at 90 s per frame in the in-house data collection, and 20 s per frame in the synchrotron data collection. The reflections were indexed using *AUTOMAR* [13]. The data collection statistics are shown in Table 2. It may be noted that the resolution of the data and their quality show no correlation with the X-ray source.

2.4. Determination of space group and data processing

The X-ray data for the four stages could be indexed almost equally well in two different space groups $P6_5$ (or $P6_1$) and $P3_2$ (or $P3_1$). In case of the space group $P6_5/P6_1$, the unit cell parameters are $a=b=17.49$ Å and $c=41.73$ Å, and the asymmetric unit is sufficient to accommodate just one dinucleotide step of a Z type helix. In case of the space group $P3_2/P3_1$, the unit cell dimensions are $a=b=\sim17.70$ Å and $c=\sim42.70$ Å with sufficient volume for a Z type tetranucleotide in the asymmetric unit. In both cases the helix would be placed such that the helix axis could coincide with the crystallographic screw axis. Overall, and at low resolution, the data indicate the space group $P3_2$ to be correct choice for data sets

Table 2
Summary of data processing and refinement statistics. Values in parentheses are for the last shell. The last row shows the root mean square deviation (Å) of helices with fiber model Z DNA [21].

Growth stages of crystal	Stage (i) hexagonal plates	Stage (ii) hexagonal plates with spots	Stage (iii) hexagonal plates with intense spots and a depression	Stage (iv) rings
Diffraction data				
Resolution (Å)	2.81 (2.91)	3.01 (3.12)	2.70 (2.80)	3.22 (3.34)
Space group	$P3_2$	$P6_5$	$P3_2$	$P3_2$
Cell constants (Å) $a=b=$	17.69	17.49	17.81	17.67
$c=$	42.49	41.73	43.00	42.72
R_{merge} (%)	6.57 (34.86)	11.09 (40.40)	4.61 (43.38)	12.68 (36.20)
Mean I/σ(I)	7.5 (1.4)	3.3 (1.0)	6.9 (1.2)	3.4 (1.2)
Completeness (%)	93 (93.9)	100 (100)	99.8 (100)	94.8 (97.5)
Multiplicity	3.22 (2.93)	6.80 (6.67)	4.44 (4.16)	3.51 (3.28)
No. of observations	1193	1035	1980	863
No. of unique reflections	343	147	426	237
Asymmetric unit	Tetranucleotide	Dinucleotide	Tetranucleotide	Tetranucleotide
Refinement				
R_{factor} (%)	24.1	19.6	24.5	23.9
R_{free} (%)	26.2	23.3	27.7	27.6
r.m.s.d. bond length (Å)	0.02	0.02	0.01	0.01
r.m.s.d. bond angle (°)	2.39	3.93	2.56	1.57
Average B Factor (Å^2)				
All atoms	27.7	23.8	42.4	54.0
Phosphate	30.9	24.4	46.5	57.4
Sugar	27.8	22.4	43.5	55.7
Bases	27.3	27.5	41.4	53.0
Water molecules	22.4	5.3	30.1	40.4
PDB entry	3UM4	3ULM	3ULN	3ULO
r.m.s.d. with fiber model of Z DNA (Å)	0.9	0.9	0.7	0.6

collected for crystals at stage (i), hexagonal plates, stage (iii), hexagonal plates crystals with intense spots and depressions, and stage (iv), fully formed ring crystals. Throughout the resolution range, hexagonal $P6_5$ has the best values of R_{merge} in the case of data collected for crystals at stage (ii), hexagonal plates with spots. These observations led to the above choice of space groups. The solution of the structures and their refinement in the respective space groups, as described below, confirmed the choice of the cell and space group.

2.5. Structure solution and refinement

Fiber models of Z type DNA were built using *INSIGHT II* [release 98.0; Biosym/MSI, San Diego, USA]. Based on the unit cell parameters and space group, molecular replacement was carried out with models using the program *Phaser* [14] of the *CCP*4 suite [15]. In case of crystals of the space group $P3_2$, the asymmetric unit contains a tetranucleotide duplex positioned on the 3_2 screw axis. The symmetry related molecules of this tetranucleotide generate the full turn of the helix. Fig. 1a shows an arbitrary full turn of a Z type DNA helix generated for crystals with the space group $P3_2$. The crystallographic 3_2 screw axis, which coincides with the helix axis of the tetranucleotide, generates an infinite disordered helix with phosphate groups having partial occupancy. Because of disorder, the tetranucleotide could stand for CpGpCpG/CpGpCpG, CpApCpG/CpGpTpG or CpGpCpA/TpGpCpG. (The presence of the A:T base-pair destroys the two-fold symmetry perpendicular to the helix axis that is present in sequences such as CGCGCG.) Due to the disorder, the tetranucleotide was constructed as TpGpTpG/TpGpTpG in which the C5 methyl group of thymine was assigned occupancy of 1/6 and N2 of guanine was assigned occupancy of 5/6.

In case of crystals of the space group $P6_5$, the asymmetric unit contains a dinucleotide step on the 6_5 screw axis. The symmetry related molecules of this dinucleotide step generate the full turn of the helix. Fig. 1b shows an arbitrary full turn of the Z type DNA helix generated for crystals with the space group $P6_5$. The crystallographic 6_5 screw axis, which coincides with the helix axis of the dinucleotide, generates an infinite disordered helix with phosphate groups having partial occupancy. Because of disorder, the dinucleotide step could stand for either CpG/CpG or CpA/TpG. (Again, the presence of the A:T base-pair destroys the two-fold symmetry perpendicular to the helix axis that is present in sequences such as CGCGCG.) Due to the disorder, the dinucleotide step was constructed as TpG/TpG where the C5 methyl group of thymine was assigned occupancy of 1/6 and N2 of guanine was assigned occupancy of 5/6.

All four models were subjected to 20 cycles of rigid body refinement and a further 5 cycles of restrained refinement in the program *REFMAC5* [16]. The structures were then refined using *REFMAC*5 with maximum-likelihood targets and the *REFMAC5* dictionary [17]. The cobalt hexammine ions could not be identified from the electron density maps. For the asymmetric unit, water molecules were added at various stages of the refinement, each time ensuring that the electron density in the (F_o–F_c) map (and in subsequent maps), as well as the temperature factors in the subsequent cycles of refinement warranted the addition. The final refinement statistics are given in Table 2. Graphical analyses of the model and the electron density maps were carried out using *Coot* [18]. PyMOL was used to prepare the figures [19].

3. Results

3.1. Crystal growth stages

Initial observations of the drop, using a Reichert-Polyvar Met2 optical microscope at a magnification of 80×, showed a clear drop. After 6 h tiny crystals were seen, which rapidly grew into large (40 μm) hexagonal plate-like single crystals in 18 h. There was no change in the appearance of the plates up to the 40th hour,

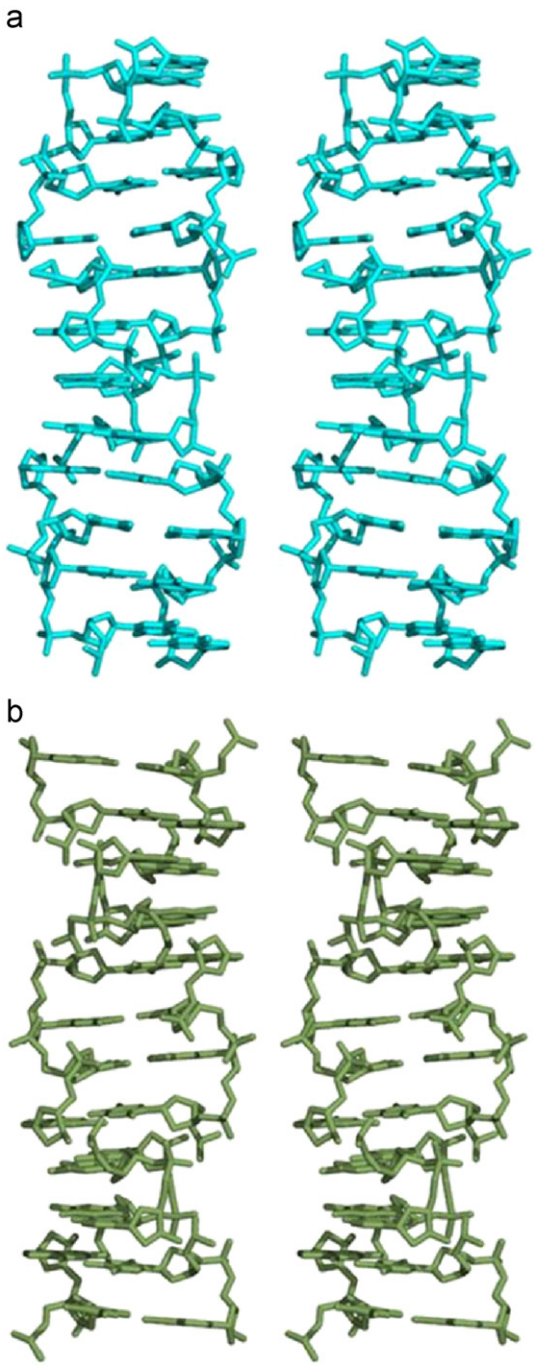

Fig. 1. Pseudo-continuous arrangement of a full turn of Z type DNA helix (stereo-view perpendicular to the helical axis) built along (a) the 3_2 screw axis using tetranucleotides in the space group $P3_2$ and (b) the 6_5 screw axis using dinucleotide step in the space group $P6_5$.

at which time the central portion of the crystal acquired a roughness that increased rapidly (Fig. 2a). The roughness was clearly due to a surface dissolution process. When we followed the growth process of one of the plates, we observed that at the 50th hour the roughness had cleared, leaving behind a distinct depression, with six sharp lines originating from the periphery and meeting at the center (Fig. 2b). Observations on another crystal in the same drop (Fig. 2e), which happened to be viewed side-on, showed that the depression occurs equally on both sides of the hexagonal plates, and that the dissolution proceeded from the two hexagonal surfaces of the crystal towards the body center of the 35 μm thick plate. The central portion of the depression then dissolved, and a small irregular hole appeared at the center of the crystal between the 91st hour and the 102nd hour. The hole expanded towards the periphery, morphing into a regular hexagon. At the 107th hour, a thick walled hexagonal ring crystal appeared (Fig. 2c). The walls gradually became thinner until, after 135 h from the start of the observations, a hexagonal ring crystal emerged in its final form (Fig. 2d). The size of the central hole, as measured by its radius, grew at varying rates from the time it first appeared. However, calculations showed that the surface area of the crystal increased linearly at the rate of $\sim$29 μm^2/h. The final stable size of the ring crystals are, on an average, outer diameter 44 μm, inner diameter 30 μm, and thickness 35 μm. These remained unaltered for more than a month when left undisturbed. A movie of the growth process is given in Supplementary Content 1.

Supplementary material related to this article can be found online at http://dx.doi.org/10.1016/j.jcrysgro.2012.05.029.

The observations of the growth stages of ring crystals (Supplementary Content 1) give insight into the process of the crystal growth, although they do not directly lead to an explanation for the mechanism of the ring formation. The observations show four main stages in the sequential growth pattern of the ring crystals: hexagonal plate, dots, depression, and hole formation. The hexagonal plate formation followed the conventional growth pattern which involves super saturation, nucleation and growth. However, the pattern of growth after this stage was different. The hexagonal plates developed dots on the surface, and then a depression was formed at the center with the disappearance of dots. At one stage, the dots disappeared completely resulting in a clear deep depression showing six lines from the vertices to the center. This depression occurred on both the sides of the crystal (Fig. 2e). When the depressions on the two sides met at the center, the hole was formed. The hole expanded out to a hexagonal shape, and formed thick walled hexagonal rings. Then the walls thinned out to form perfect ring shaped crystals. To establish that these were ring crystals with holes and not an artifact of a particular view of the crystal, a glass fiber was inserted through the hole (Fig. 2f).

In our earlier report of the ring crystals [12] we had speculated on possible growth patterns, and had suggested either a six-fold twinning mechanism, or a template directed process as being responsible for the shape. The present observations indicate that ring crystals grow through a dissolution process that begins at the center of a perfectly 'normal' crystal. A similar process of dissolution of the core is thought to be responsible for hexagonal ring crystals of size about 5 μm of the mineral osarizawaite [6]. The forces involved in the formation of inorganic crystals are different from, and usually stronger than, those involved in the formation of biomolecular crystals. Thus, the growth processes of ring crystals of the two types of molecules are probably different.

3.2. Overall structure

Overall, the crystal structures of the four stages mentioned above fall within the Z DNA family [20]. The two strands of the duplexes form anti parallel left handed helices with the Watson–Crick base pairing. The phosphate groups follow a zigzag left handed spiral. The helices possess a dinucleotide repeat with deep minor grooves and flat major grooves. The torsion angle χ is *anti* for all the pyrimidine bases and *syn* for all the purine bases, as in regular Z DNA. Similarly, the sugar puckering alternates between a conformation close to C3′ endo for the purines and one close to C2′ endo for the pyrimidines. In the present structure, most of the backbone adopts the Z_I conformation [20]. Comparison of the root mean square deviation (Table 2) of these Z type DNA helices with the fiber model [21] shows that the structures are similar (r.m.s.d. < 1 Å). Despite the fact that the X-ray diffraction data were collected from crystals in different stages of ring

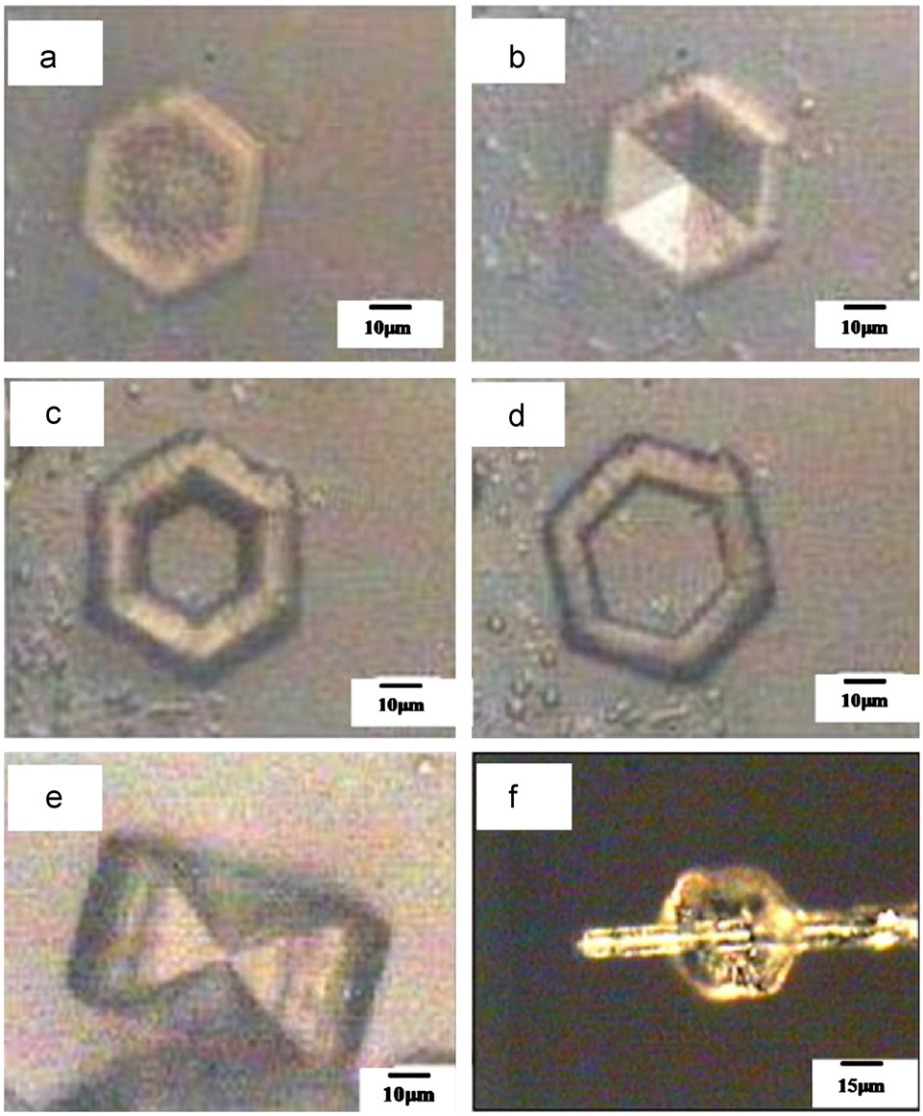

Fig. 2. Growth of oligonucleotide ring crystals: (a) roughness on the surface, (b) depression with vertical lines, (c) hexagonal hole, (d) thin-walled ring crystal, (e) side view of depression on both sides and (f) ring crystal with a thin glass fiber inserted through the hole at the center.

formation, the overall structures of the helices remain the same i.e. of the Z type DNA. There is no correlation between the morphological changes occurring in the crystal and those of the overall structure of the DNA molecules.

An interesting observation, however, is the average thermal factor (*B*) that progressively increases (Table 2) from stage (ii) to stage (iv). This may indicate that during ring formation, the helical atoms (especially the backbone atoms) vibrate due to frustration in the close helical packing [1]. Thus, the increase in average thermal factor from stages (ii) to (iv) may be due to subtle changes in the nascent crystalline ground state where presence of negative charges on the backbone phosphate groups leads to frustration in the packing interactions, inhibiting arrangements of helices that arise by simple translations in directions perpendicular to the helix axis [1]. However, owing to the disorder present in the crystals and the low resolution of the data, detailed differences, if any, could not be analyzed.

3.3. Helical packing

The gross packing motif of all four crystal structures remains the same, i.e. hexagonal close packing arrangement of cylinders. There are a total of 65 Z DNA structures with deposited coordinates in the Nucleic acid Data Bank [22], 51 of which belong to the orthorhombic space groups such as $P2_12_12_1$, and 8 structures that belong to hexagonal space groups such as $P6_5$ and $P6_522$. The rest are either monoclinic $P2_1$ (5) or triclinic P1 (1). Most of the hexamers are in the space group $P2_12_12_1$; the packing mode is called the 'mode 1', previously, termed as the 'magnesium form' [23], since Mg^{2+} ions contribute to the stability of this type of packing. However, later experiments showed that the presence of magnesium is not essential for mode 1 packing. A few hexamers, octamers and decamers crystallize in the hexagonal space group; the packing mode is called the 'mode 2', previously called the 'spermine form' [24], since polyamines such as spermine or cobalt hexamine stabilize this type of packing. Again, later structures showed that Z DNA can adopt mode 2 packing even in the presence of magnesium [25]. The two packing modes have different patterns of contacts between symmetry related Z DNA double helices in the crystal. The present hexamer crystallizes in the mode 2 in all four crystal structures. We thus infer that the morphological changes involved in transformation of the hexagonal 'normal' crystals to hexagonal 'ring' crystals are not due to any discernible changes in the helical packing.

4. Discussion

Rings crystals of DNA were first reported by us [12] for the non-palindromic oligonucleotide sequences d(CGCGCA). d(TGCGCG) and d(CGCACG).d(CGTGCG). These ring crystals were grown in the presence of cobalt hexamine chloride for the former sequence, and ruthenium hexamine chloride for the latter sequence. The sequences were designed as part of a systematic crystallographic study to explore the effect of the introduction of A:T base pairs in sequences that otherwise consisted of alternating C:G base pairs [20], which are known to favor left-handed Z type helices [20,26]. The design of the sequences we studied was based upon the canonical hexamer $d(CGCGCG)_2$ [20,27]. Since this sequence is self-complementary, the duplex has a dyad, and there are only three ways in which a single A:T base pair could replace one of the G:C pairs. We have studied all three possibilities in various conditions of salt, pH, temperature, etc (Table 3). However, as reported previously [12] and in the present study, ring-shaped crystals grew only in the presence of cobalt or ruthenium hexamine chloride, and then only in a specific range of concentrations.

Several palindromic sequences such as $d(CGCG)_2$, $d(CGCGCG)_2$, $d(CGCGCGCG)_2$, $d(CCCGGG)_2$ and $d(CGTACGTACG)_2$ crystallize as Z type DNA with similar packing patterns ([32–34], PDB ID 239D [35]). These crystals have been grown in a variety of different conditions, including in the presence of cobalt or ruthenium hexamine chloride [33,35]. Ring-shaped crystals have not been reported in any of these cases.

From Table 1, it is clear that the concentration of hexamine chloride plays a crucial role in the formation of ring crystals. When the concentration is low, nucleation does not occur. When the concentration is too high, the DNA precipitates, and again no crystals are formed. Concentrations greater than about 0.5 mM of the metal ion, but less than about 0.75 mM, favor crystallization. These crystals, which grow as hexagonal plates, soon dissolve from the center to form rings. We may speculate that the formation of the initial crystals leads to a depletion of the metal ion in the solution, which facilitates the gradual dissolution from the center, leading to the ring-shaped crystals. This, of course, will increase the metal ion concentration in the solution once again, but regrowth of the central portion of the dissolved crystal is presumably prevented by the geometry. Thus the ring crystals, once formed, preserve their shape. It is not clear why only cobalt and ruthenium hexammine should have this effect. Unfortunately, the metal ion could not be identified in the crystal structures reported in the present manuscript. In the literature, there are reports of the structures of $d(CGCGCG)_2$ and $d(CGCGCA)\cdot d(TGCGCG)$ in which the position of the hexammine ion are identified [30,31,33]. However, we are unable to find any clues in these structures which may contribute to an explanation regarding the connections between the formations of ring crystals on the one hand, and the metal ion, its concentration and the sequence of the oligomers, on the other.

As discussed in the Section 1, it has been shown in [1] that when DNA helices bundle together, as for example in the formation of DNA fibers, the presence of negative charges on the backbone phosphate groups leads to frustration in the packing interactions, inhibiting arrangements of helices that arise by simple translations in directions perpendicular to the helix axis. Adjacent helices are arranged such that contacts between phosphate groups are minimized, unless mediated by cations. The optimal arrangement would differ depending on the type of helix. This implies that in the case of oligonucleotide crystals, the crystal system and symmetry adopted would depend on the helix type, the metal ion concentration and the length of the oligonucleotide helix. It has been observed that crystals of Z type hexamers, especially of the three sequences mentioned above often show degeneracy in space group [36], and the X-ray diffraction pattern of such crystals may be indexed with almost equal felicity in many different space groups. Most commonly, the best choice, decided on the basis of the R_{merge}, is orthorhombic $P2_12_12_1$ or hexagonal $P6_5$, with the higher symmetry being correlated in some cases with lower ion concentration in the crystallization drop [37]. (It may be noted that in almost all these cases the crystal habit remains the same—i.e., hexagonal plates.) In the hexagonal space group, however, alternate columns of helices are situated so that the helical axis coincides with the crystallographic 6_5 screw axis, leading to translational disorder of this column along the helix axis, or equivalently, rotational disorder about the helix axis. Since the space group and crystal

Table 3
Summary of systematic crystallographic studies of the introduction of A:T base pairs in hexamer sequences that consisted of C:G base pairs. The crystallization attempts were carried out with constant pH (6.9) of the buffer (sodium cacodylate trihydrate) and at room temperature (293 K).

Sequence (5′–3′)	Conc. of counter ions (mM)	Diffraction data collection temperature (K)	Crystal habit	Resolution (Å)	Space group	Ions bound to DNA	PDB IDs and references
d(C**A**CGCG)·d(CGCG**T**G)	24.00 mM Mg^{2+}	296	Hexagonal shaped crystals	1.60	$P2_12_12_1$	–	181D [28]
d(C**A**CGCG). d(CGCG**T**G)	1.00 mM $Ru(NH_3)_6^{3+}$	296	Hexagonal shaped crystals	1.64	$P2_12_12_1$	–	351D [29]
d(C**A**CGCG). d(CGCG**T**G)	12.00 mM Ba^{2+}	100	Rectangular prism-like crystals	1.72	$P2_1$	Ba^{2+}	4E4O[a]
d(C**A**CGCG). d(CGCG**T**G)	10.00 mM Ba^{2+}	100	Rectangular prism-like crystals	1.67	$P2_12_12_1$	Ba^{2+}	4E2R[a]
d(C**A**CGCG). d(CGCG**T**G)	5.00 mM Ba^{2+}	100	Hexagonal shaped crystals	1.86	$P6_5$	Ba^{2+}	4E60[a]
d(C**A**CGCG). d(CGCG**T**G)	10.00 mM Mn^{2+}	100	Rectangular prism-like crystals	1.61	$P2_1$	Mn^{2+}	4DWY[a]
d(C**A**CGCG). d(CGCG**T**G)	1.00 mM Mn^{2+}	100	Hexagonal shaped crystals	1.76	$P6_5$	Mn^{2+}	4DY8[a]
d(C**A**CGCG). d(CGCG**T**G)	0.50–0.75 mM $Co(NH_3)_6^{3+}$	100	Hexagonal rings formed	2.81, 3.01, 2.70, 3.22	$P3_2$, $P6_5$	–	3UM4[b], 3ULM[b], 3ULN[b], 3ULO[b]
d(CGC**A**CG). d(CG**T**GCG)	10.00 mM Ba^{2+}	296	Hexagonal shaped crystals	2.50	$P2_1$	–	180D [28]
d(CGCGC**A**). d(**T**GCGCG)	0.50 mM $Co(NH_3)_6^{3+}$	296	Hexagonal prism-shaped crystals	1.71	$P2_12_12_1$	$Co(NH_3)_6^{3+}$	1XA2 [30]
d(CGCGC**A**). d(**T**GCGCG)	0.30 mM $Co(NH_3)_6^{3+}$	296	Hexagonal prism-shaped crystals	1.86	$P6_5$	$Co(NH_3)_6^{3+}$	1XAM [30]
d(CGCGC**A**). d(**T**GCGCG)	0.80 mM $Ru(NH_3)_6^{3+}$	296	Hexagonal shaped crystals	1.54	$P2_12_12_1$	$Ru(NH_3)_6^{3+}$	2HTO [31]
d(CGCGC**A**). d(**T**GCGCG)	0.40 mM $Ru(NH_3)_6^{3+}$	296	Hexagonal shaped crystals	2.60	$P6_5$	$Ru(NH_3)_6^{3+}$	2HTT[a]

[a] Unpublished results from our lab.
[b] Present article.

symmetry arise from the packing interactions (and not vice versa), we may perhaps infer that in such cases the scarcity of mediating ions leads to frustration in the packing and consequently the observed disorder.

Our conclusions are in agreement with previous experimental studies on DNA condensates [38,39] which reveal that crystalline structures maintain hexagonal ordering at lower density, whereas at higher densities the hexagonal order gives way to an orthorhombic ground state. Thus even without the full knowledge of the inter-molecule forces at play in this morphological transition, we can note that the ground states of the packing of DNA helices will largely fall into two classes, frustrated (energetically less favored) and unfrustrated (energetically favored) [2]. The symmetry of the former is hexagonal, while the latter possesses only rhombohedral symmetry.

Acknowledgments

We thank Prof. V. Ravichandran, Department of Nuclear Physics, University of Madras, for use of the microscope. This work was financially supported by the following agencies of the Government of India: DBT under a research Grant and DST under the FIST program. We gratefully acknowledge the use of the Synchrotron facility at Elettra, Trieste, Italy, under the program of DST. PKM and SV thank CSIR for Senior Research Fellowships.

References

[1] G.M. Grason, Europhysics Letters 83 (58003) (2008) p1–p6.
[2] V.A. Bloomfield, Current Opinion in Structural Biology 6 (1996) 334–341.
[3] W. Gelbert, R. Bruinsma, P. Pincus, V. Parsegian, Physics Today 58 (2000) 38–44.
[4] R.A.M. Scott, M.G. Jarvis, Journal of Crystal Growth 16 (1972) 82–85.
[5] V. Gantcheva, S. Simov, P. Kamadjiev, M. Gospodinov, Journal of Materials Science 10 (1975) 1943–1946.
[6] E.H. Nickel, American Mineralogist 65 (1980) 1287–1290.
[7] G. Attolini, C. Paorici, P. Ramasamy, Journal of Crystal Growth 78 (1986) 181–184.
[8] S.R. Dickinson, K.M. McGrath, Journal of Materials Chemistry 13 (2003) 928–933.
[9] Y. Oaki, H. Imai, Crystal Growth and Design 3 (2003) 711–716.
[10] W.F. Berg, Proceedings of the Royal Society of London Series A—Mathematical Physical and Engineering Sciences 164 (1938) 79–95.
[11] S. Amelinckx, D. Bernaerts, X.B. Zhang, G. van Tandeloo, J. van Landuyt, Science 267 (1995) 1334–1338.
[12] P.S. Kumar, N. Gautham, Current Science 77 (1999) 1076–1078.
[13] K.S. Bartels, C. Klein, The AUTOMAR Manual. v.1.4, Norderstedt, Germany: MAR Research GmbH, 2003.
[14] A.J. McCoy, R.W. Grosse-Kunstleve, P.D. Adams, M.D. Winn, L.C. Storoni, R.J. Read, Journal of Applied Crystallography 40 (2007) 658–674.
[15] Collaborative Computing Project, Number 4, Acta Crystallographica D50 (1994) 760–763.
[16] G.N. Murshudov, A.A. Vagin, E.J. Dodson, Acta Crystallographica D53 (1997) 240–255.
[17] A.A. Vagin, R.A. Steiner, A.A. Lebedev, L. Potterton, S. McNicholas, F. Long, G.N. Murshudov, Acta Crystallographica D60 (2004) 2184–2195.
[18] P. Emsley, K. Cowtan, Acta Crystallographica D60 (2004) 2126–2132.
[19] W.L. DeLano, The PyMOL Molecular Graphics System, DeLano Scientific, San Carlos, California, USA, 1998.
[20] A.H.-J. Wang, G.J. Quigley, F.J. Kolpak, J.I. Crawford, J.H. van Boom, G. van der Marel, A. Rich, Nature 282 (1979) 680–686.
[21] S. Arnott, R. Chandrasekaran, D.L. Birdsall, A.G.W. Leslie, R.L. Ratliff, Nature 283 (1980) 743–745.
[22] H.M. Berman, W.K. Olson, D.L. Beveridge, J. Westbrook, A. Gelbin, T. Demeny, S.-H. Hsieh, A.R. Srinivasan, B. Schneider, Biophysical Journal 63 (1992) 751–759.
[23] R.V. Gessner, C.A. Frederick, G.J. Quigley, A. Rich, A.H.-J. Wang, Journal of Biological Chemistry 264 (1989) 7921–7935.
[24] M. Egli, L.D. Williams, Q. Gao, A. Rich, Biochemistry 30 (1991) 11388–11402.
[25] M.H. Moore, L. van Meervelt, S.A. Salisbury, P.K.T. Lin, D.M. Brown, Journal of Molecular Biology 251 (1995) 665–673.
[26] A.H.-J. Wang, G.J. Quigley, F.J. Kolpak, J.H. van Boom, G. van der Marel, A. Rich, Science 211 (1981) 171–176.
[27] P.K. Mandal, S. Venkadesh, N. Gautham, Journal of the Indian Institute of Science 88 (2008) 73–93.
[28] C. Sadasivan, N. Gautham, Journal of Molecular Biology 248 (1995) 918–930.
[29] P. Karthe, N. Gautham, Acta Crystallographica D54 (1998) 501–509.
[30] S. Thiyagarajan, S.S. Rajan, N. Gautham, Nucleic Acids Research 32 (2004) 5945–5953.
[31] D. Bharanidharan, S. Thiyagarajan, N. Gautham, Acta Crystallographica F63 (2007) 1008–1013.
[32] J.L. Crawford, F.J. Kolpak, A.H.-J. Wang, G.J. Quigley, J.H. van Boom, G.A. van der Marel, A. Rich, Proceedings of the National Academy of Sciences USA 77 (1980) 4016–4020.
[33] P.S. Ho, C.A. Frederick, D. Saal, A.H.-J. Wang, A. Rich, Journal of Biomolecular Structure and Dynamics 4 (1987) 521–534.
[34] S. Fuji, A.H.-J. Wang, G.J. Quigley, H. Westerink, G.A. van der Marel, J.H. van Boom, A. Rich, Biopolymers 24 (1985) 243–250.
[35] R.G. Brennan, E. Westhof, M. Sundaralingam, Journal of Biomolecular Structure and Dynamics 4 (1986) 649–665.
[36] C. Sadasivan, P. Karthe, N. Gautham, Acta Crystallographica D50 (1994) 192–196.
[37] S. Thiyagarajan, S.S. Rajan, N. Gautham, Acta Crystallographica D61 (2005) 1125–1131.
[38] D. Durand, J. Doucet, F. Livolant, Physics II France 2 (1992) 1769–1783.
[39] F. Livolant, A. Leforestier, Progress in Polymer Science 21 (1996) 1115–1164.